AD-A131 924   NOVEL TECHNIQUES FOR ENHANCED REFLECTIVITY INFRARED   1/1
                MIRRORS(U) COLORADO STATE UNIV FORT COLLINS DEPT OF
                PHYSICS J R SITES JUL 83 AFWL-TR-83-13
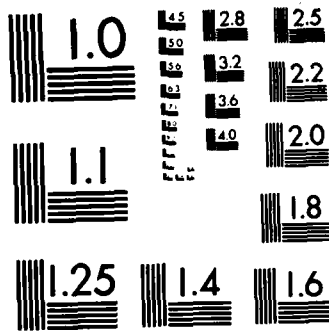UNCLASSIFIED   F29601-82-K-0009   F/G 7/4   NL

END
FILMED
DTIC

MICROCOPY RESOLUTION TEST CHART

NATIONAL BUREAU OF STANDARDS-1963-A

②

AD A131924

NOVEL TECHNIQUES FOR ENHANCED REFLECTIVITY INFRARED MIRRORS

James R. Sites

Colorado State University
Department of Physics
Fort Collins, CO   80528

July 1983

Final Report

DTIC
SELECTE**D**
AUG 2 9 1983

B

DTIC FILE COPY

83   08   22   096

This final report was prepared by the Colorado State University, Fort Collins, Colorado, under Contract F29601-82-K-0009, Job Order 317J0849 with the Air Force Weapons Laboratory, Kirtland Air Force Base, New Mexico. Captain Myron T. Maclin (ARAO) was the Laboratory Project Officer-in-Charge.

When Government drawings, specifications, or other data are used for any purpose other than in connection with a definitely Government-related procurement, the United States Government incurs no responsibility or any obligation whatsoever. The fact that the Government may have formulated or in any way supplied the said drawings, specifications, or other data, is not to be regarded by implication, or otherwise in any manner construed, as licensing the holder, or any other person or corporation; or conveying any rights or permission to manufacture, use, or sell any patented invention that may in any way be related thereto.
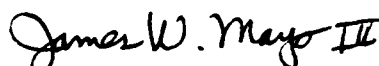
This report has been authored by a contractor of the United States Government. Accordingly, the United States Government retains a nonexclusive, royalty-free license to publish or reproduce the material contained herein, or allow others to do so, for the United States Government purposes.

If your address has changed, if you wish to be removed from our mailing list, or if your organization no longer employs the addressee, please notify AFWL/ARAO, Kirtland AFB, NM 87117 to help us maintain a current mailing list.
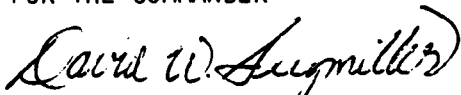
This report has been reviewed by the Public Affairs Office and is releasable to the National Technical Information Service (NTIS). At NTIS, it will be available to the general public, including foreign nations.

This technical report has been reviewed and is approved for publication.

Myron J Maclin

MYRON T. MACLIN
Captain, USAF
Project Officer

FOR THE COMMANDER

James W. Mayo III   *David W. Seegmiller*

JAMES W. MAYO III   DAVID W. SEEGMILLER
Lt Colonel, USAF   Colonel, USAF
Chief, Advanced Resonator/Optics Br   Chief, Advanced Laser Technology Div

DO NOT RETURN COPIES OF THIS REPORT UNLESS CONTRACTUAL OBLIGATIONS OR NOTICE ON A SPECIFIC DOCUMENT REQUIRES THAT IT BE RETURNED.

REPORT DOCUMENTATION PAGE		READ INSTRUCTIONS BEFORE COMPLETING FORM
1. REPORT NUMBER AFWL-TR-83-13	2. GOVT ACCESSION NO. AD-A131 924	3. RECIPIENT'S CATALOG NUMBER
4. TITLE *(and Subtitle)* NOVEL TECHNIQUES FOR ENHANCED REFLECTIVITY INFRARED MIRRORS		5. TYPE OF REPORT & PERIOD COVERED Final Report
		6. PERFORMING ORG. REPORT NUMBER IXL
7. AUTHOR(s) James R. Sites		8. CONTRACT OR GRANT NUMBER(s) F29601-82-K-0009
9. PERFORMING ORGANIZATION NAME AND ADDRESS Colorado State University Department of Physics Fort Collins, CO 80528		10. PROGRAM ELEMENT, PROJECT, TASK AREA & WORK UNIT NUMBERS 63605F/317J0849
11. CONTROLLING OFFICE NAME AND ADDRESS Air Force Weapons Laboratory (ARAO) Kirtland Air Force Base, NM 87117		12. REPORT DATE July 1983
		13. NUMBER OF PAGES 42
14. MONITORING AGENCY NAME & ADDRESS*(if different from Controlling Office)*		15. SECURITY CLASS. *(of this report)* Unclassified
		15a. DECLASSIFICATION/DOWNGRADING SCHEDULE

16. DISTRIBUTION STATEMENT *(of this Report)*

Approved for public release; distribution unlimited.

17. DISTRIBUTION STATEMENT *(of the abstract entered in Block 20, if different from Report)*

18. SUPPLEMENTARY NOTES

19. KEY WORDS *(Continue on reverse side if necessary and identify by block number)*

Ion Beam	Laser Damage	Epitaxy
SiO_2	Optical Absorption	Photoassisted Deposition
Ta_2O_5	Stress	Chemical Vapor Deposition
TiO_2	Thin Films	
Reflectivity	Refractive Index	

20. ABSTRACT *(Continue on reverse side if necessary and identify by block number)*

Three types of thin films for high reflectivity mirror applications have been deposited and characterized. High and low refractive index oxide films deposited by ion beam sputtering have low optical absorption and sound mechanical properties. Refractory metal films produced by laser photodissociation display good reflectivity. Chemical vapor deposition of ZnSe layers has been used to explore the crystalline structures possible with different substrates and growth parameters.

DD ＦＯＲＭ 1473 EDITION OF 1 NOV 65 IS OBSOLETE
1 JAN 73

PREFACE

Personnel at Colorado State University and others contributed to the deposition program. Graduate students, Paul Gilstrap and Rong Rujkorakarn, and undergraduate, Rod Hannum, worked with the Principal Investigator, Professor James Sites, on the ion beam deposition and evaluation. Mr. Gilstrap used his work as the basis of his Master of Science thesis. Raj Solanki worked with Professor George Collins on the photoassisted deposition, and graduate student, Sri Sritharan, with Professor Kenneth Jones on the chemical vapor deposition. At Kirtland AFB, Ed Miesak and Dr. Alan Stewart performed the laser damage tests. At the Optical Coating Laboratories, Inc., Jerry Dodds and Dr. Thomas Allen did the high resolution optical absorption measurements. Back at CSU, Kent Geib and Art Nelson did the Auger and X-ray photoelectron spectroscopy measurements. The contribution of each is greatly appreciated. Professor Jones is particularly appreciated for his assistance in the report preparation.

Accession For	
NTIS GRA&I	✔
DTIC TAB	☐
Unannounced	☐
Justification	
By	
Distribution/	
Availability Codes	
	Avail and/or
Dist	Special
A	

1/2

CONTENTS

I. INTRODUCTION

This report describes the results of novel deposition techniques for thin film optical coatings with applications to high reflectivity laser mirrors. The work was motivated by the observation that coatings being used in high-power applications have some limitations with respect to porosity, mechanical integrity, and long-term optical degradation.

The three areas explored are: (1) Ion beam sputter deposition of oxide coatings. This technique has been successful in several electronics applications and with mirrors for ring gyro lasers. (2) Deposition of refractory metals using laser dissociation of metal-radical complexes. This procedure allows fast low temperature deposition over specified areas. (3) Chemical vapor deposition of zinc sulfide and zinc selenide. This technique is within a few degrees of thermal equilibrium, and the resulting films are strongly dependent on the substrate surface structure.

In each area of exploration, the purpose was to identify the advantages and drawbacks of the films actually deposited and those that could be made under more ideal conditions. Emphasis in this exploratory phase was on macroscopic properties of the films; relatively little was done with atomic structure. The results are described in the following section; conclusions and recommendations are given in Section III.

II. EXPERIMENTAL PROGRAM

1. ION BEAM SPUTTER DEPOSITION

High refractive index TiO_2 and Ta_2O_5 layers and low index SiO_2 layers were deposited by ion beam sputtering (Ref. 1). In this technique, a columnated beam of monoenergetic ions strikes a target and the sputtered atoms impinge and stick on a nearby substrate. Typically the ion beam energy is the order of 1000 eV and the ion flux 1-2 mA/cm^2, leading to energies near 20 eV for the sputtered atoms, and film growth rates the order of 100 Å/min. Refinements to the deposition process include the addition of reactive ions, such as oxygen, to the beam, and the use of a second beam aimed at the substrate for precleaning or film growth modification.

There are several potential advantages to ion beam sputter deposition. Because of relatively high impingement energy of the sputtered atoms, films are expected to be dense and relatively impervious to environmental factors such as water vapor. From an analysis point of view, the ion beam sputter technique is very attractive in that each deposition parameter can be varied independently of the others and it is relatively convenient to identify and possibly modify the critical parameter.

Coating materials selected were somewhat similar to one another, all oxides, and thus amenable to similar sputtering procedures. SiO_2 and TiO_2 layers have been used for low and high index optical coatings by several groups interested in high-power laser mirrors (Ref. 2,3). Ta_2O_5 is a less common optical material, but also has a refractive index above 2.

a. <u>Apparatus</u> -- The ion beam sputter deposition apparatus used is shown in Figure 1. The vacuum system was constructed to order by CHA Industries and the primary ion source by Ion-Tech, Inc. A stainless steel vacuum chamber, 35.5 cm in diameter and 33 cm long, is capped by hinged doors which allow easy access to the fixturing inside.

The primary ion source is mounted on one door. It is a broad beam Kaufman-type source of a design originally developed for space propulsion
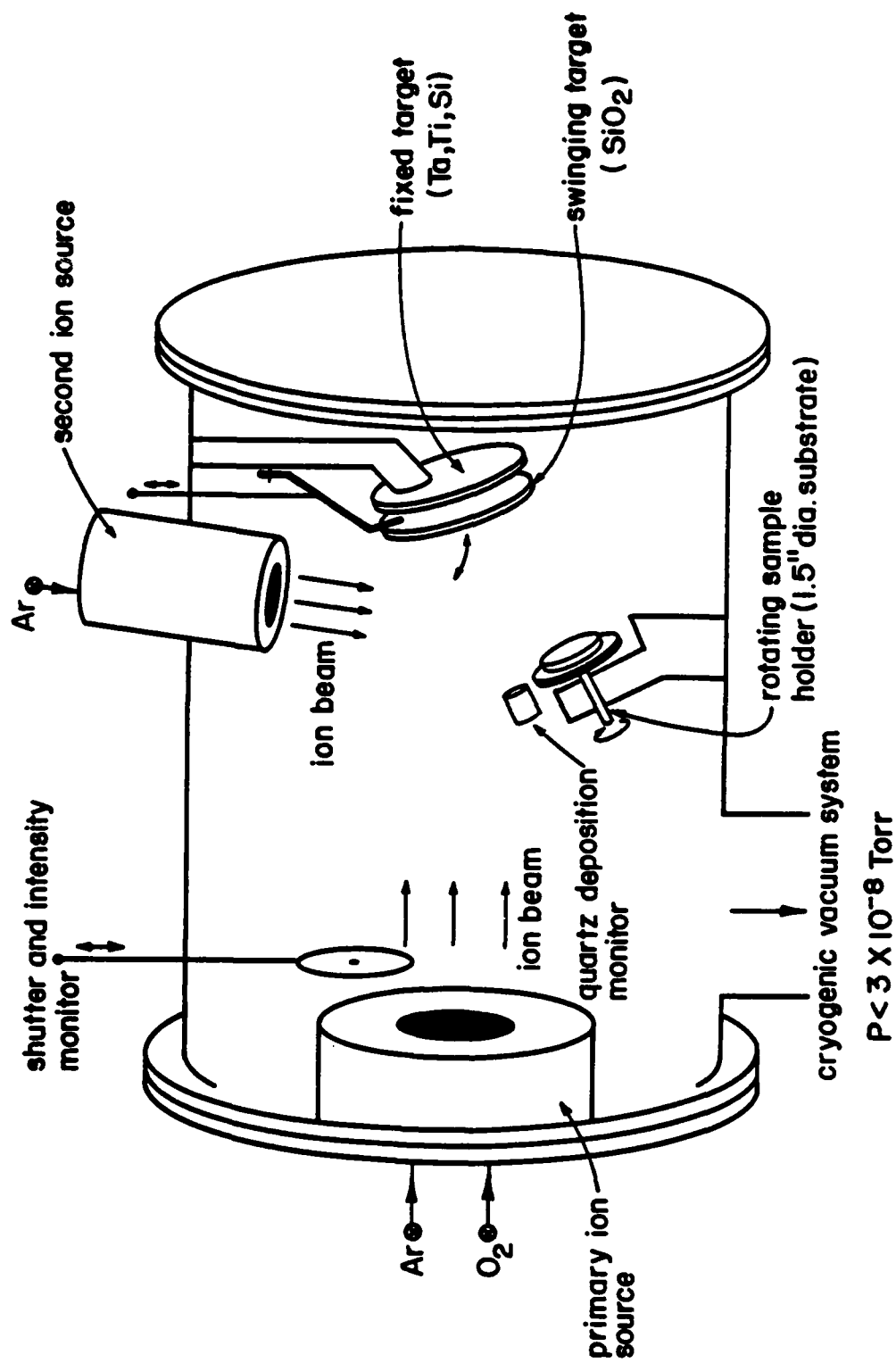
Figure 1. Ion beam sputter deposition apparatus (from Ref. 1).

7

(Ref. 4). It produces a 5-cm-diameter beam of monoenergetic ions, either argon or an argon/oxygen mixture for the depositions described in this report. The beam is neutralized with electrons from a hot filament to minimize beam divergence and charging of the target.

A water-cooled target holder is mounted 20 cm downstream from the ion source. Actual targets are round or square plates, 0.1 to 1.0 cm thick, 12-15 cm in lateral dimension. The normal to the target is oriented at a 55° angle with respect to the primary ion beam. For multi-layer films a second target can be swung into the beam path just in front of the first target.

Substrates for deposition are mounted on a rotating sample holder placed 10 cm from the target with its face parallel to the target. The sample holder can accommodate substrates up to 4 cm in diameter. Several interchangeable mounts are available for the different sized substrates used. Small test sample mounts and a quartz deposition monitor are placed adjacent to the rotating substrate holder.

A second ion source is mounted on the top of the vacuum chamber, and its beam is directed onto the substrate itself. This beam is 3 cm in diameter at the source and diverges to 4 cm at the substrate. Its purposes are to sputter clean the substrate prior to deposition, and to possibly modify film stress through substrate bombardment during deposition. The current density of the second ion beam is 0.1 mA/cm^2 and energy of the ions is set to 200-300 eV. This source is used only with argon.

b. <u>Deposition</u> -- In ion beam sputter deposition of oxides, there is a choice to be made between using an oxide target or an elemental one. In either case oxygen must be added during the sputtering process. With an oxide target, a 90:10 partial pressure mixture of argon and oxygen is found to work well. With an elemental target of Si, Ti, or Ta, the percentage of oxygen must be at least 25% to form films with low optical absorptance. Oxygen was added through the primary beam for all the results described in this report. There does not appear to be a definitive choice between the oxide and the elemental targets. The elemental targets are generally available in higher purity (99.999%) and sputter approximately 30% faster.

8

However, the greater oxygen requirement of the elemental target shortens filament lifetimes from about 15 to 5 hours. In practice, an arbitrary choice was made to use elemental targets for TiO_2 and Ta_2O_5 and an oxide target for SiO_2.

Several types of substrates were used for the oxide coating, because of requirements for different types of analysis. The substrates used are listed in Table 1.

TABLE 1. SUBSTRATES USED FOR ION BEAM SPUTTER DEPOSITION OF OXIDE COATINGS

Property to be Analyzed	Substrate	Size
Transmission and reflection Refractive index	Microscope slide	2.5 × 7.5 cm
Calorimetric optical absorption	Fused silica	1.27 cm diam. × 0.06 cm thick
Laser damage tests	Fused silica	3.86 cm diam. × 1.27 cm thick
Internal stress	Glass cover slip	1.8 cm diam. × 180 μm thick
X-ray photoelectron spectroscopy (XPS, or ESCA)	Silicon wafer	Irregular

Substrate cleaning was judged to be a critical part of the ion beam sputter deposition program. Cleaning before the substrates were mounted in the vacuum chamber concentrated on removal of particulate contaminants. No strong reagents were used. The substrates were first ultrasonically cleaned in a deionizing detergent for a relatively brief period of one minute. They were then flushed with hot flowing tap water and with flowing deionizing water. The final step to remove particulates was a drag cleaning with lens tissue wetted with filtered acetone. Filtering the acetone was found to be more important than which grade of acetone was used. Also important was the practice of dragging the lens tissue slowly and not allowing any acetone to remain on the substrate in liquid form. Particle counts on substrates cleaned in this fashion were the order of $5/cm^2$ prior to deposition. Even

9

though the entire deposition facility was maintained in clean room conditions of 200 airborne particles greater than 0.5 μm in diameter per cubic foot $(7000/m^3)$, the particle count embedded in the films regularly rose from the $5/cm^2$ before deposition to about $50/cm^2$ after deposition.

After the substrate, or group of substrates, is mounted in the vacuum chamber, the roughing and cryopumping cycle takes approximately 30 minutes to reach a pressure of about 10^{-7} torr (10^{-5} Pa). A mixture of argon and oxygen from standard high purity cylinders is then bled into the pr ʾry source at a rate of approximately 0.3 sccm. The resulting backgro   pressure then rises to $8x10^{-5}$ torr (10^{-2} Pa).

The primary ion source is activated by first forming a magnet: ʾ .ld enhanced gas discharge between anode and cathode. Approximately 40 ᵥ is required. The grid voltage is slowly increased to its operating voltage, generally 1000 V, and the neutralizer is adjusted to give zero net charge in the beam as determined by a Faraday cup monitor.

Initially the primary beam is used only to sputter clean the target. It is assumed that 5 minutes of sputtering at 1000 eV is sufficient to remove any surface contamination. Next, the primary beam is turned off, and the secondary beam is activated to clean the substrate surface. In this case a lower energy, 500 eV, is used for about five minutes. The reasoning behind the lower energy is that the substrate is relatively clean after the external procedures described above and that a higher energy would be more likely to damage the surface. The primary difference observed between substrates that are sputter cleaned and those that are not is that the film adhesion as determined by a Sebastian tester is always greater than 10,000 psi (70 MPa) on sputter cleaned substrates and often a factor of 10 less on those that are not sputter cleaned.

Actual deposition takes place next with the secondary ion source turned off, except in the stress modification experiment described below, and the primary beam restored to 1000 eV and 1.5 mA/cm^2. Deposition rates are approximately 60 Å/min., slightly less with an oxide target. The target temperature typically rises to about 200°C despite the water cooling and the substrate temperature to about 100°C. Most of the single films

10

deposited were designed to have an optical thickness of one-half wavelength at 1.06 µm, or a physical thickness of 2100 to 3500 Å depending on refractive index. Thus deposition times ranged from 35 to 60 min. After deposition, the ion source is turned off, the vacuum chamber is backfilled with pure nitrogen gas and allowed to stand for a few minutes, and the sample is removed.

c. Film Thickness -- Physical thickness of the sputter deposited films was measured with a Talysurf surface profiling instrument. For accurate results it is necessary to form a sharp step between the level of the substrate and the level of the deposited film. Initial steps formed by blocking the depositing flux with a shadow mask (Fig. 2a) were found to have rounded corners. An innovation was to make a line on the substrate with a standard, permanent ink transparency marking pen, deposit the film, and remove the film above the ink by dissolving the ink in acetone. The result, as seen in Figure 2b, is a much sharper profile and a thickness resolution of 50 Å.

Thickness uniformity was achieved by measuring the thickness of a film on a large non-rotated substrate at several points, as illustrated in Figure 3a. The rotating substrate holder was then placed in the most linear appearing part of the profile, just to the left of center as defined in Figure 3a. The resulting thickness profiles across two films on rotated 3.9 cm diameter substrates are shown in Figure 3b. The spread in thickness for the thicker film is about 60 Å, for the thinner one closer to 30 Å, essentially the instrument resolution in both cases.

Optical thickness of the single layer films was determined from the wavelengths of the maxima and minima in the reflection spectra. As a practical matter, the difference between the first minimum and 1.06 µm was taken as the primary measure of how close the film was to being half-wavelength.

d. Refractive Index -- The refractive index n of single layer oxide films was determined from the maximum values of the reflectivity R_m near 1 µm:

11

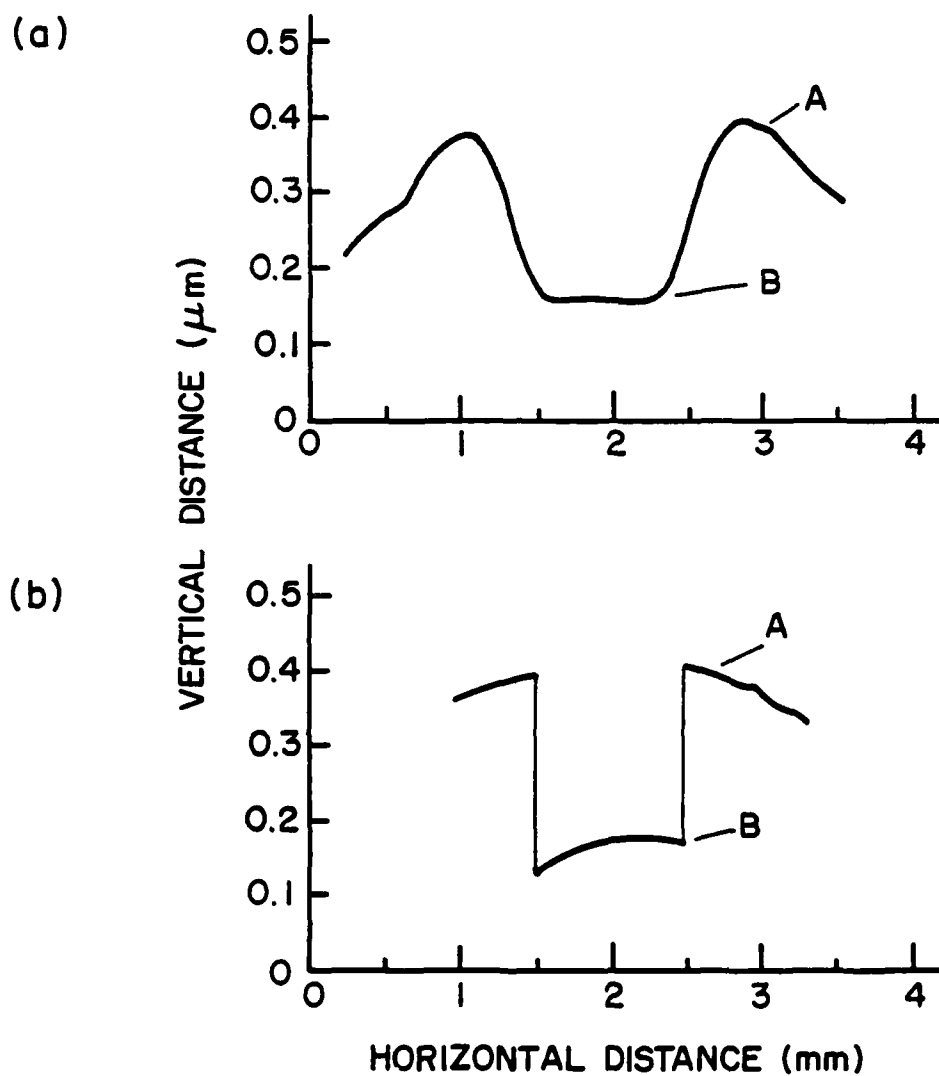Figure 2. Film thickness determination using the Talysurf profiling instru-
ment. (a) Step in film using a shadow mask. (b) Step in film
using a transparency pen; ink later dissolved with acetone. A
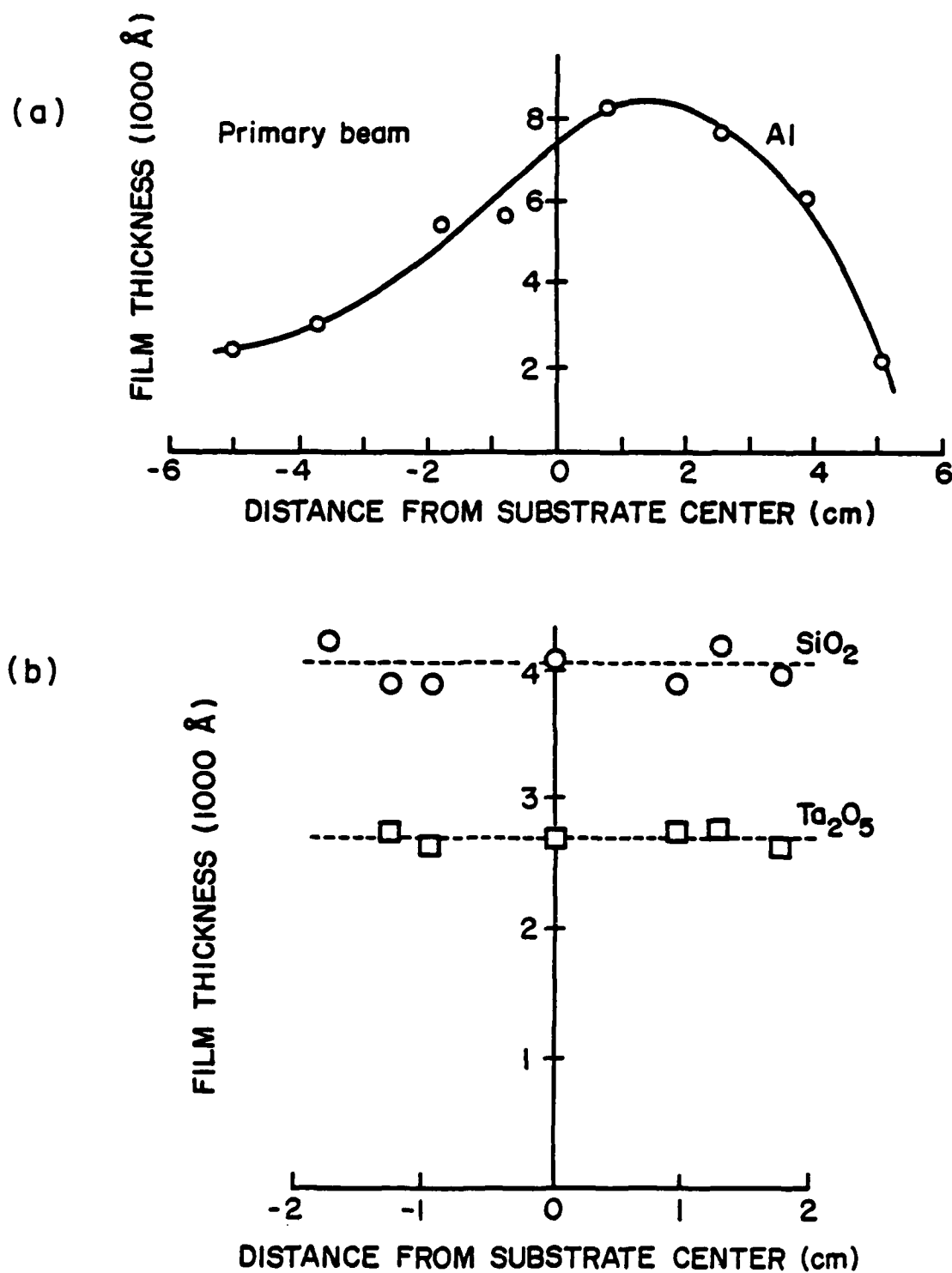denotes the level of the film, B the level of the bare substrate.

Figure 3. (a) Thickness profile of a large, non-rotated substrate.

(b) Thickness profile of a 3.9-cm-diameter substrate, rotated during deposition.

13

$$n = [n_s(1 + \sqrt{R_m})/(1 - \sqrt{R_m})]^{1/2} \qquad (1)$$

where n_s is the substrate index, assumed to be 1.56 for the glass used. The values from the maximum reflectivity on either side of 1 μm were found to differ by no more than 3% and were averaged. The resulting indices are given in Table 2. Also given in Table 2 are the values determined from the transmission spectrum. In the latter case, it was assumed that the absorption was less than 1% and R_m was found by subtracting the transmissivity from 1. In retrospect the second procedure is considered more reliable because the direct reflectivity measurements involved a comparison of the near specular reflection from the deposited film with diffuse reflection from the standard.

TABLE 2. REFRACTIVE INDICES OF DEPOSITED FILMS

Type of Film	Index from Reflection Spectrum	Index from Transmission Spectrum
SiO_2	1.48 ± 0.02	1.50 ± 0.02
Ta_2O_3	2.03 ± 0.03	2.12 ± 0.03
TiO_2	2.27 ± 0.05	2.50 ± 0.05

e. Composition and Structure -- Composition of the oxide films was determined by X-ray photoelectron spectroscopy, often referred to as ESCA. The energy spectrum of electrons emitted when the surface was bombarded with X rays was measured, the peaks were identified, and the published scaling factors were applied (Ref. 5). All films deposited with sufficient oxygen, as discussed above, were reasonably close to the expected stoichiometry as seen in Table 3. The films as a whole seem to be slightly oxygen deficient, but the resolution precludes a definitive statement. Insufficient oxygen in the beam clearly reduced the oxygen content of the SiO_2 films, deposited from an oxide target, by as much as 10%. The oxygen in the metallic target films could be reduced essentially to zero. The only contaminant found in the films was carbon. A large surface concentration

14

of carbon (10%) is thought to be picked up through handling and transport. It was reduced to the 1% resolution of the XPS measurement after a light sputter etch.

TABLE 3.   FILM COMPOSITION FROM XPS MEASUREMENTS

Film	Expected Composition		Measured Composition	
SiO_2	Si	33%	Si	34 ± 2%
	O	67	O	66 ± 2
			C	0 ± 1
Ta_2O_5	Ta	28	Ta	30 ± 2
	O_2	72	O	69 ± 2
			C	1 ± 1
TiO_2	Ti	33	Ti	34 ± 2
	O	67	O	65 ± 2
			C	1 ± 1

The films are assumed to be structurally amorphous, but there is currently no conclusive evidence. An argument can be made that sputtered atoms impinging on a near room temperature substrate (100°C) at energies the order of 20 eV are likely to orient themselves randomly. Surface migration is possible, but only at considerably higher temperatures (Ref. 6). Scanning electron microscopy and X-ray diffraction at CSU showed no evidence of crystallites, but in both cases a null result could simply indicate the experiment was not done with sufficient care.

f.   Internal Stress -- Mechanical stress of deposited films is a major concern in any coating work. A novel, but simple and effective technique utilizing geometric optics has been developed (Ref. 7). The curvature of a thin microscope cover slip (18 mm diameter x 0.18 mm thick) is measured as shown in Fig. 4. The cover slip is placed on an optically flat mirror and is illuminated through a partially transparent mirror. Two images are formed on a projection screen, one from the perimeter of the cover slip blocking the optical flat, the second from reflection from the curved
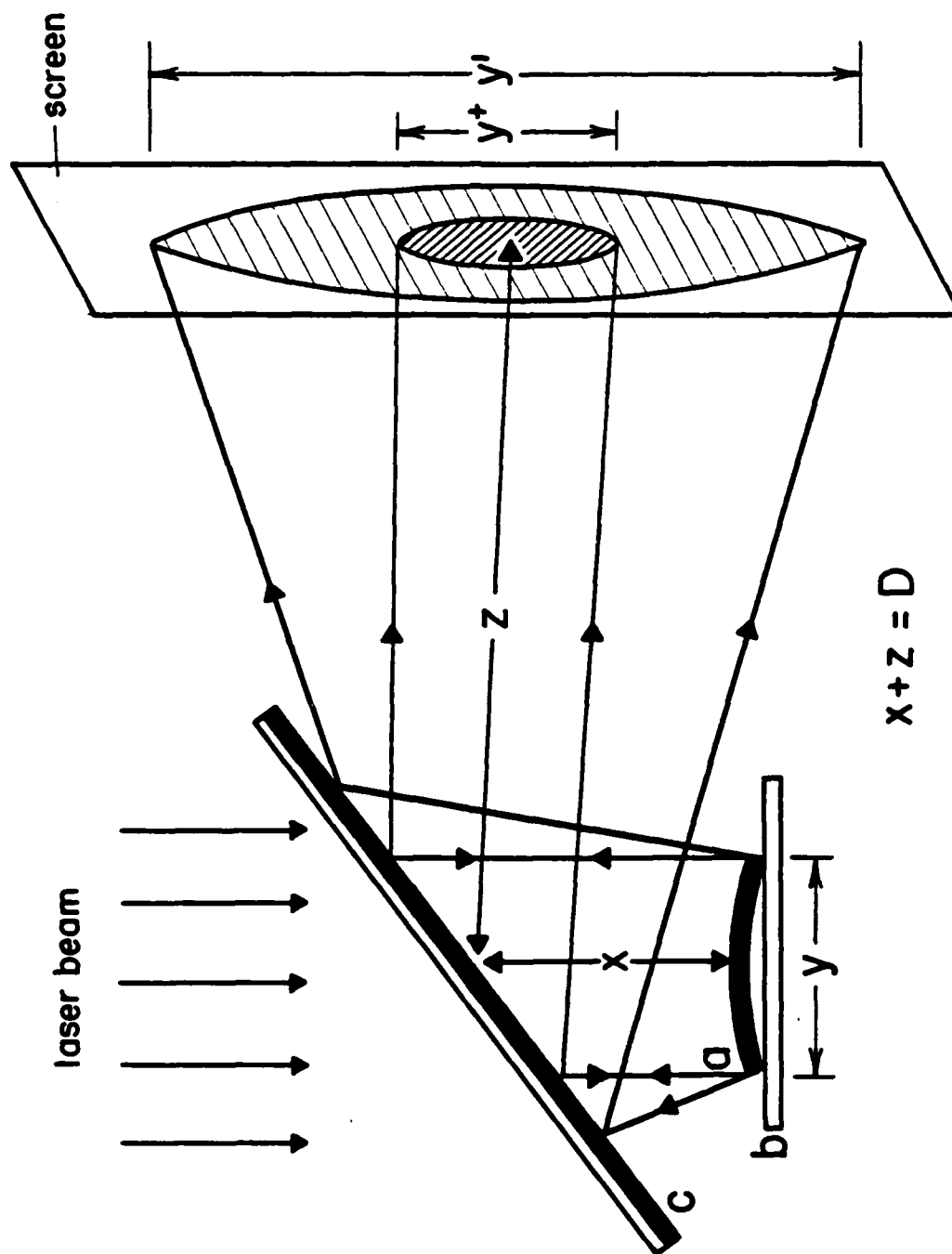
15

Figure 4. Schematic of geometric optics curvature measurement, showing cover slip (a), reflecting optical flat (b), and partially transmitting mirror (c) (from Ref. 7).

surface of the cover slip. Assuming that the laser beam has only a small divergence, the radius of curvature r is related to image sizes by

$$r \simeq \frac{2yD}{y' - y^+} \tag{2}$$

where the lengths are defined in Fig. 4. By measuring the radius of curvature before (r_0) and after (r) deposition, film stress S can be calculated by (Ref. 8)

$$S = \frac{Ed^2}{6(1-\nu)t} \left(\frac{1}{r} - \frac{1}{r_0}\right) \tag{3}$$

where t is the film thickness, d is the substrate thickness, E the Young's modulus of the substrate, and ν the Poisson ratio of the substrate.

Values of E and ν were supplied by Corning, the cover slip manufacturer. However, an independent measurement of the relation between stress and curvature seemed desirable, and the apparatus shown in Fig. 5 was constructed. A cover slip was deliberately bowed by subjecting it to a known partial vacuum, and the curvature was measured directly with the Talysurf profilometer. The direct calibration agreed with the calculated values.

Stress was measured for all three deposited oxides, and the results are shown in Fig. 6. The stress was always found to be compressive. It was greatest in the SiO_2 layers. Attempts to lower the stress through substrate bombardment with the secondary ion beam were only partially successful. The larger SiO_2 stress was reduced about 20%; that of Ta_2O_5 was essentially unchanged.

g. Optical Absorption -- The optical absorption of several ion-beam-sputter deposited films was measured by the Optical Coating Laboratories, Inc. (OCLI). The instrument used was an absorption calorimeter in which a temperature increase is measured when the film on a fused silica substrate is exposed to 1.06 μm radiation. The system has a resolution of 2 p/m. Absorption results are given in Table 4. All the films had thicknesses close to half-wavelength.
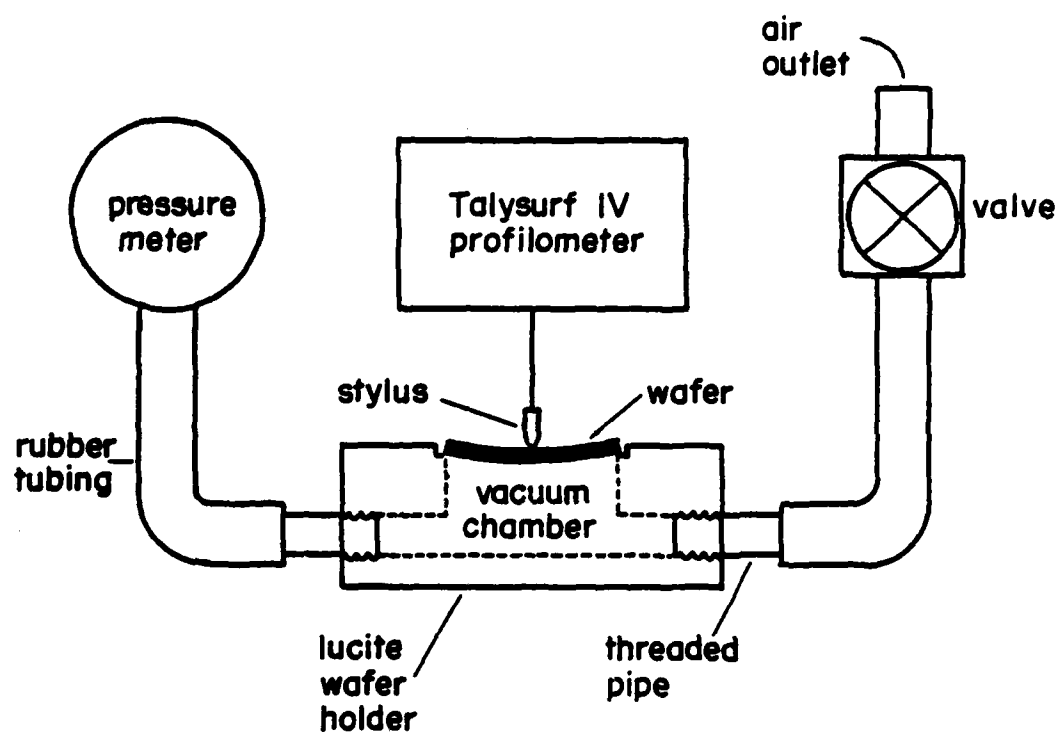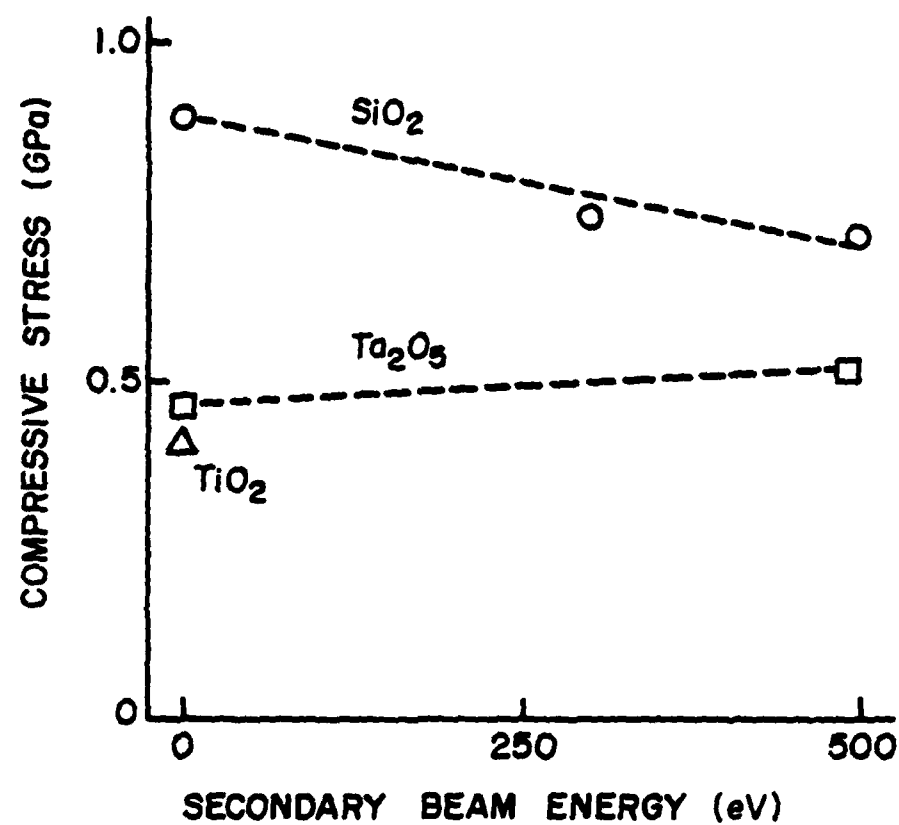
Figure 5. Apparatus to relate stress to curvature.

Figure 6.   Stress in single layer films showing the effect of substrate
bombardment with a second ion beam.   Beam density was 0.1 mA/cm^2
(from Ref. 1).

19

TABLE 4. OPTICAL ABSORPTION RESULTS

Sample	Film Type	Thickness	O_2 Partial Pressure During Deposition	Absorptance	Absorption Coefficient
NWC-2	SiO_2	3800 Å	0%	501 p/m	18 cm^{-1}
NWC-3	SiO_2	4650	35	77	2.3
NWC-4	SiO_2	3900	50	79	2.8
NWC-5	Ta_2O_5	2450	50	79	3.9
NWC-6	Ta_2O_5	3000	25	119	5.0
NWC-7	Ta_2O_5	2650	65	.124	5.5
NWC-8	TiO_2	2300	50	381	18
NWC-9	TiO_2	2400	25	446	21
NWC-9*	TiO_2	2400	25	385	18

The SiO_2 films were found to have absorptance slightly less than 100 p/m, the Ta_2O_5 slightly above 100 p/m. TiO_2 absorptance was about 4 times higher. One sample (NWC-2) made by sputtering an SiO_2 target without added oxygen was found to have an absorptance substantially higher than the other SiO_2 films. One of the TiO_2 films was baked at 250°C in air for four hours to possibly drive off water vapor, a procedure that, according to Dr. Allen at OCLI, often reduces the absorptance of porous films. Results after the bake, marked by an asterisk, indicate relatively little improvement, implying that water vapor trapped in porous material is not likely the cause of the higher absorptance.

h. Multilayer Films -- A small number of quarter-wave three-layer films, Ta_2O_5 - SiO_2 - Ta_2O_5 and TiO_2 - SiO_2 - TiO_2, were fabricated by changing targets at appropriate times as described earlier. The three-layer films were designed for maximum reflectivity at 1.06 µm, and the measured reflectivity spectrum for a Ta_2O_5 based three-layer stack is shown in Fig. 7. Also shown for comparison is the calculated spectrum based on the matrix calculation technique (Ref. 9). Refractive indices were taken from the values deduced for single layers.

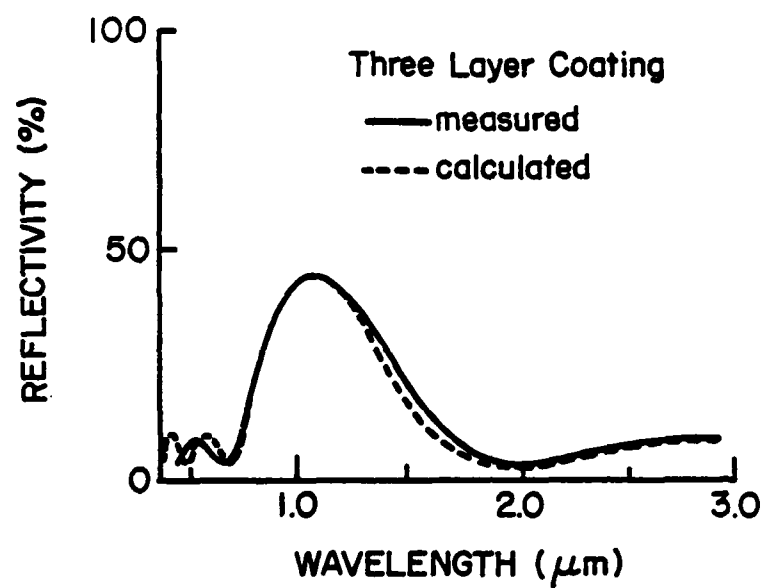Extensive calculations have also been made to study the effect of

Figure 7. Comparison of calculated and measured reflectivities for quarter-wave Ta_2O_5 - SiO_2 - Ta_2O_5 coating (from Ref. 1).

variations in thickness of one of the layers in a multilayer coating
(Ref. 10). As can be seen in Fig. 8, the maximum reflectivity for a three-
layer coating changes very little, but the secondary maxima and minima are
strongly affected. The values of calculated reflectivity at three secondary
extremes, as defined in Fig. 8d, can be plotted against thickness error for
each of the three layers. These curves, shown in Fig. 9, allow one to take
values from measured reflectivity spectra and determine which layer thick-
ness needs to be adjusted.

The same procedure can be applied to any number of film layers.
Figure 10 shows the general features for 15-layer films. Again the maximum
reflectivity is essentially unaffected. In Figure 10a the outer layer is
altered and the envelope of secondary structure changes markedly. In
Figure 10b, the effect of having all the high index layers altered with
respect to the low index ones leads to a strong reflection maximum at one-
half the primary peak's wavelength. The BASIC language computer code for
generating the reflection curves is included as an appendix to this report.

i. **Laser Induced Damage** -- Laser damage tests were performed at the
Air Force Weapons Laboratory (AFWL) on each type of coating deposited. The
test procedure was to expose the coating to a single laser pulse and to
compare microscope pictures of the impact region taken before and after the
pulse. Any visible change was designated as damage. The laser wavelength
was 1.06 µm, pulse duration was 5 ns, and the 1/e radius of the beam was
130 µm. The laser pulse energy was varied from 0.03 J to 0.6 J, each pulse
directed to a different area on the coating. Approximately 20 pulses of
varying energies were used during the earlier tests, over 100 in the later
ones.

Results of the damage tests are shown in Fig. 11. The solid boxes
denote the lower laser energy densities where damage was never observed, and
the dashed boxes the energy densities where damage was sometimes observed.
The single-layer films were all approximately half-wavelength thick, and
the three-layer coatings were one-quarter wavelength for each layer. The
energy densities shown in Fig. 11 are scaled downward from those originally
reported. The change was due to new information supplied by AFWL concern-
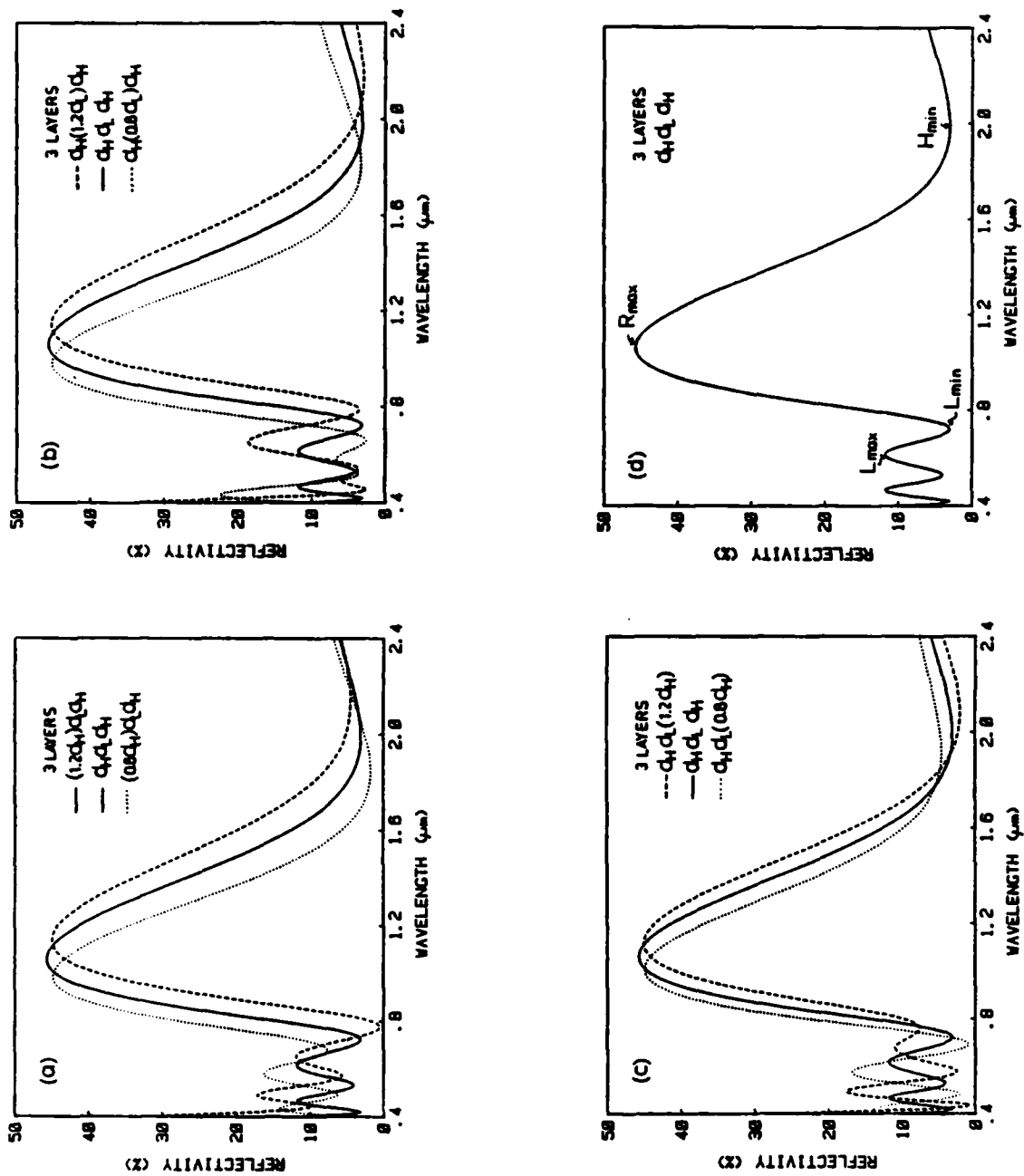ing the laser beam profile.

22

Figure 8. Calculated reflectance spectra for thickness variations of: (a) the outer layer, (b) the middle layer, (c) the inner layer, and (d) with no variations. ($d_H = 1.06/4n_H$ μm, $d_L = 1.06/4n_L$ μm where $n_H = 2.03$, $n_L = 1.48$) (from Ref. 10).

23

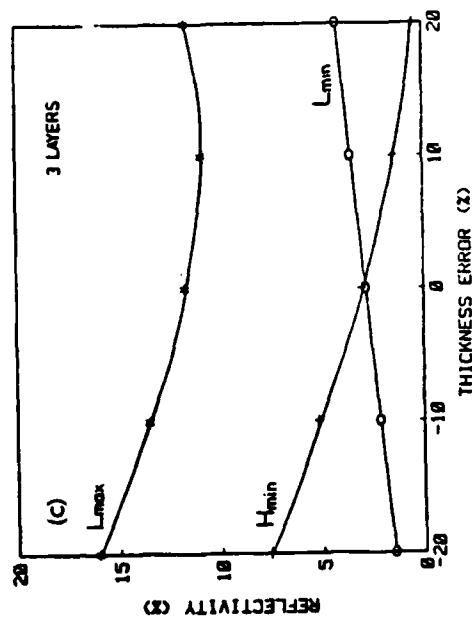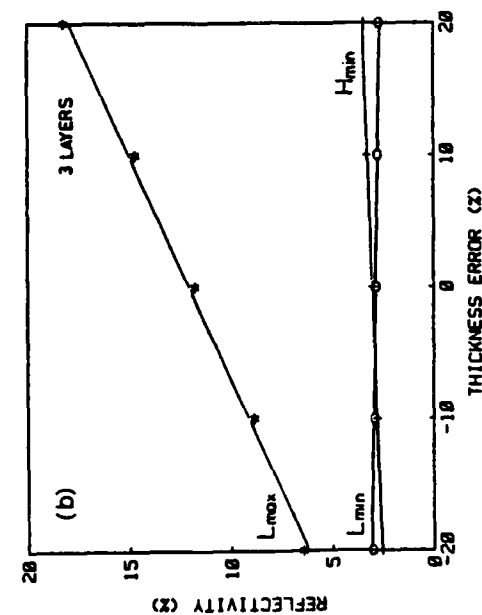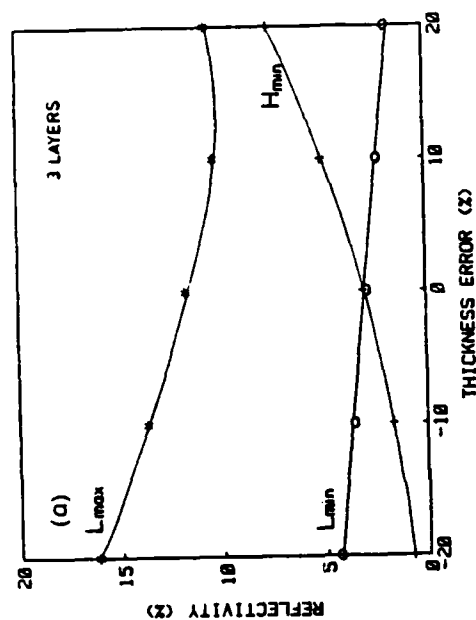Figure 9. Reflectances of the secondary features vs. thickness deviation of: (a) the outer layer (b) the middle layer, and (c) the inner layer (from Ref. 10).
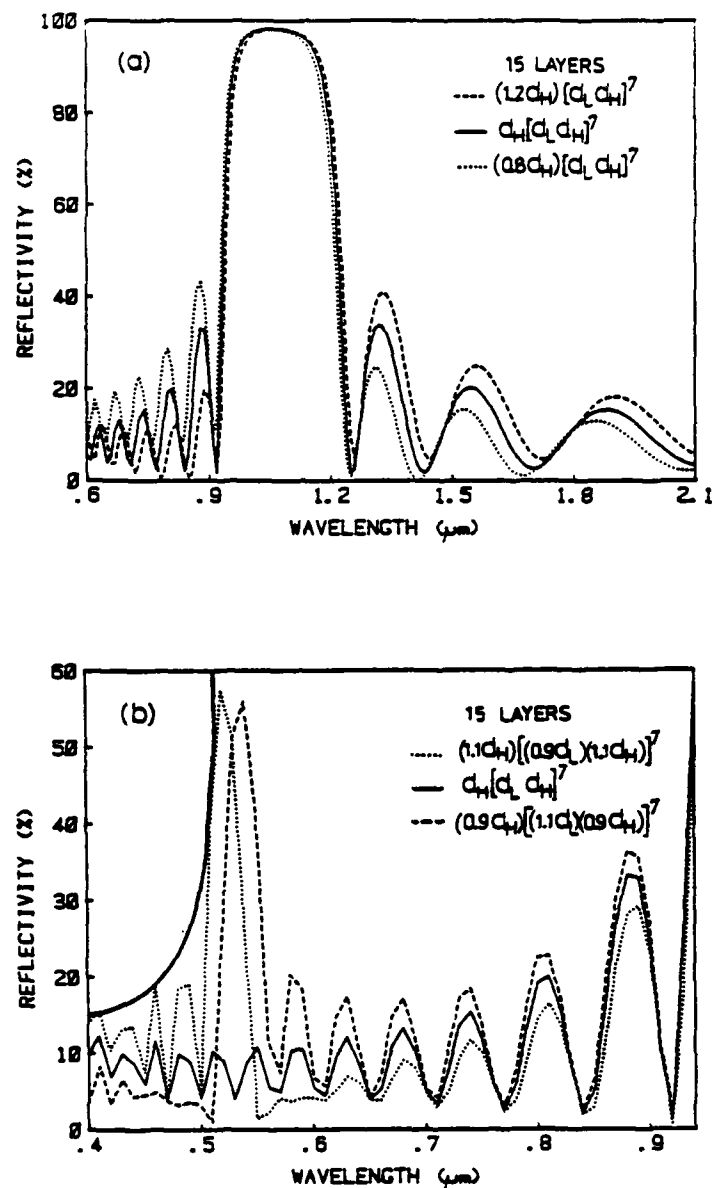
24

Figure 10. Calculated reflectance spectra of a fifteen layer coating when
(a) only the outer layer thickness is altered (by 20%), and
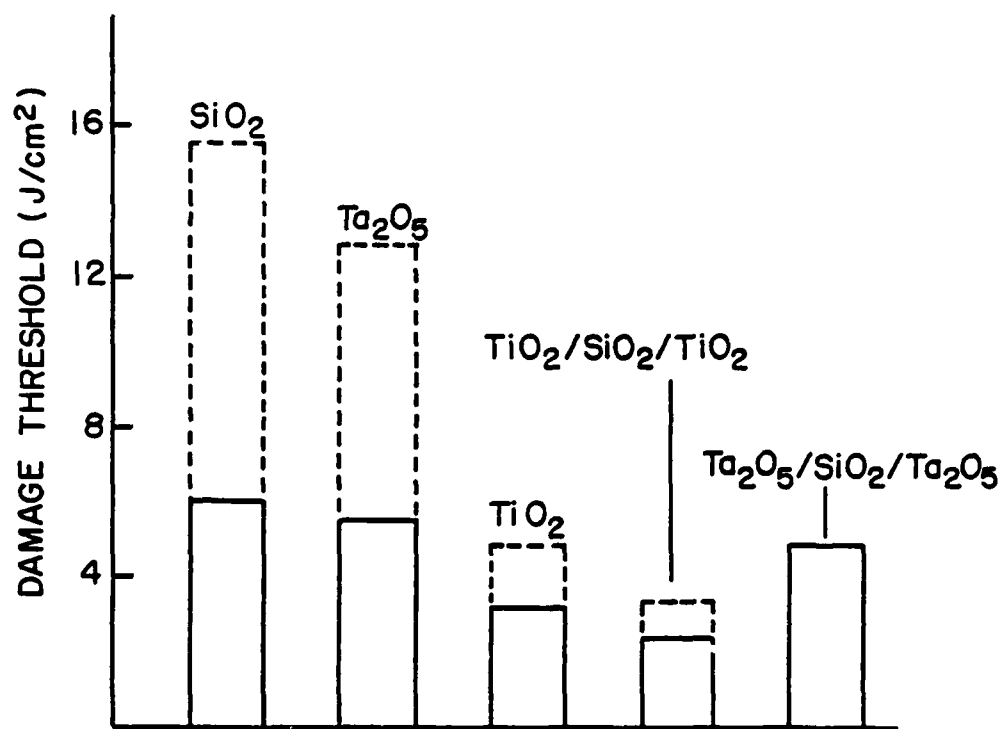(b) all the layer thicknesses are altered (each by 10%)
(from Ref. 10).

Figure 11.   Laser induced damage thresholds.

Most of the damage observed in the dashed box energy density regions in Fig. 11 occurred near the residual visible defects, or light scattering sites, described earlier. At present the nature of these scattering sites is not known. Their presence, however, is the likely cause of the large spread in energy density threshold observed with several of the coatings.

2. PHOTOASSISTED DEPOSITION

Photoassisted deposition was used to form layers of tungsten, molybdenum, and chromium, all potential candidates for smooth, damage-resistant mirror surfaces (Ref. 11). The procedure is to use an ultraviolet laser to photodissociate metal-hexacarbonyls, $W(CO)_6$, $Mo(CO)_6$, and $Cr(CO)_6$. If the dissociation takes place near an appropriate substrate, then the metallic atoms will adhere, forming in many cases a smooth reflective surface. Dissociation of metal-hexafluorides was also used for deposition, but was abandoned due to the damage the residual fluorine caused to the vacuum system seals.

The apparatus for the photoassisted deposition is shown in Fig. 12. The laser used for photodeposition was an eximer laser (Lumonics TE-860), which could be operated at several UV wavelengths. The substrates for the photodeposited films were either silicon, quartz, or glass. They could be placed either perpendicular to the laser beam as shown, or at a grazing angle. An important feature of the apparatus shown is the flow of helium gas across the window where the laser beam enters, necessary to prevent deposition on the windows. The carbonyl reservoir and the connecting tube were both heated to the vicinity 50°C with heating tape to produce a flow of the metal-carbonyl. The lens outside the chamber was divergent so that the laser beam covered a substrate area approximately 2 cm in diameter.

Typical deposition times were 100 s, and the resulting thicknesses were 3000-4000 Å. Prior to deposition oxygen was introduced to the chamber and the laser turned on to induce oxidation of surface contaminants. This procedure seemed to improve adhesion of the deposited films. Initial films were deposited with 193-nm light from ArF transitions. These photons have energy of 6.4 eV which was chosen to be intermediate between the estimated 3 eV needed to dissociate the carbonyl from the metal, but less than the 9 eV
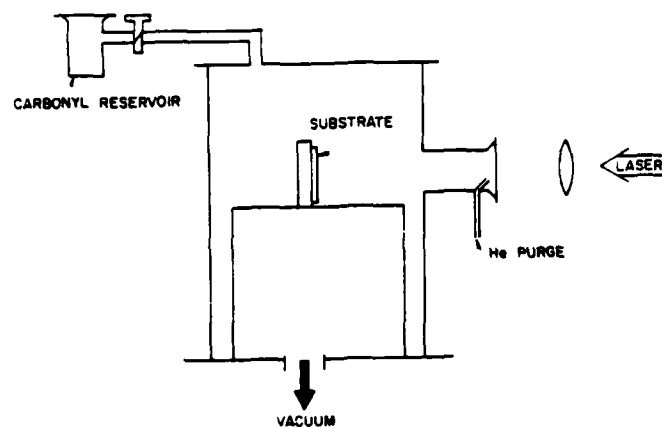
27

Figure 12. Experimental arrangement for photoassisted deposition of
refractory metal films (from Ref. 11).

thought to break the C-O bonds. These first films were found to have low
reflectivities and large carbon and oxygen impurities. Subsequent films,
therefore, were deposited using 248-nm (5.0-eV) photons from KrF transitions
and seemed to be of higher quality.

Results for three of the photoassisted deposition films are given in
Table 5. Reflectivity results were hampered by film coverage only mar-
ginally as large as the spectrophotometer beam and from some errors in oper-
ation. After the improvement with the lower energy photons, they were
typically 5-10% below reported bulk reflectivities (Ref. 12) in the visible.
Stress was tensile and the same order of magnitude as the compressive stress
in the ion-beam-sputtered oxide films. Adhesion was good, again at the
limit of the Sebastian tester used.

TABLE 5. PHOTOASSISTED DEPOSITION RESULTS

Metal	Thickness	Deposition Rate	Reflectivity at 6328 Å	Tensile Stress	Adhesion
Mo	4000 Å	2500 Å/min	51	0.3 GPa	55 MPa
W	3000	1700	55	0.2	65
Cr	3500	2000	48	0.7	50

Compositional analysis of the metallic films was accomplished with
Auger spectroscopy. The primary impurity found was oxygen (5-7%), which was
attributed to the relatively crude vacuum system used. Carbon was also
observed, in concentrations of a few percent with the 193-nm wavelength
laser, less than 1% at 248 nm. No other impurity was seen. The oxygen level
in the films was virtually the same with either laser wavelength, strongly
suggesting that its origin was not the same as the carbon, but probably
residual O_2 in the system.

Films deposited with the laser beam striking the substrate at a grazing
angle were markedly different from the relatively shiny films described above.
The grazing angle films appeared quite black. Microscopic inspection
revealed that the surface of these films was quite rough, in sharp contrast

to the smooth surfaces of the films deposited with a normal incidence beam. No studies were made of polarization or beam intensity effects on the black films.

3. CHEMICAL VAPOR DEPOSITION

Zinc selenide films have been grown using the metalo-organic (MO-CVD) process. ZnSe is a wide band-gap semiconductor that is frequently used as the high index material in highly reflecting dielectric mirrors (Ref. 13). There are also applications of ZnSe for blue and green emitting phosphors (Ref. 14, 15) and for blue emitting LEDs (Ref. 16, 17).

Films have been grown using direct sublimation (Ref. 13, 18, 19), evaporating zinc and mixing it with H_2Se (Ref. 20, 21), iodine transport CVD (Ref. 22), LPE (Ref. 23), MBE (Ref. 24), and MO-CVD (Ref. 25-28). A major disadvantage of using the sublimation technique is that the constituent partial pressures are not individually controlled. As a result, the films tend to be zinc rich because the vapor pressure of selenium is much higher. Also, the thickness control is not good since the constituent flows cannot be abruptly turned off. The major disadvantage of evaporating zinc and mixing it with H_2Se is that high mixing (1000°C) and deposition (700°C) temperatures are required to produce high quality films. When these films are deposited on a GaAs substrate, an intermediate compound such as Ga_2Se_3 can form. The chemical reactions involved in iodine transport CVD are complex and difficult to control, and the deposition temperatures are again relatively high. The LPE-grown films are not high quality films, and the MBE technique is not yet sufficiently developed to be economically feasible on a mass production basis.

The MO-CVD technique is attractive because high-quality films can be deposited at relatively low (350°C) temperatures (Ref. 27), the constituent vapor pressures are individually controlled, and the thickness control is excellent since the zinc and selenium containing vapors can be abruptly turned off. The primary disadvantage is that upon mixing there is a room temperature reaction, presumably a hydrogen elimination reaction, in which a larger molecule with a much lower vapor pressure is formed and precipitates out of the gas flow. Studies elsewhere (Ref. 26, 27) have overcome

30

this problem by using a low-pressure, high-flow-rate system, and Blanconnier, et al. (Ref. 25) have partially overcome this problem by mixing the constituents together very near the substrate surface. The former method requires a relatively complex system, but the homogeneity is poorer using the latter method.

In the current work, the problems associated with the room temperature reaction were alleviated by forming the adduct, $(C_2H_5)Zn \cdot Se(C_2H_5)$ by mixing diethylzinc (DEZ) and diethylselenide (DES) prior to introducing the H_2Se. The DEZ is not now free to form the adduct $(C_2H_5)Zn \cdot SeH_2$ which can react via a hydrogen elimination reaction.

Single crystal films were grown on (100) GaAs substrates oriented 2° toward the [110] direction, and polycrystalline films were grown on thin glass cover slides. The GaAs substrates were prepared in a way similar to that of Stutius (Ref. 27). This includes boiling in TCE, an acetone rinse followed by a rinse in DI water, etching for 30 s in a 5:1:1 solution of H_2SO_4, H_2O_2, and H_2O, boiling in HCl followed by a DI rinse, and blow drying in N_2. The cover glass slides were washed with acetone, rinsed in methanol, rinsed in DI water, etched in 10% HF, rinsed in DI water, and blow dried in N_2. Prior to deposition, the curvature of the disk was measured by placing in on an optical flat and counting the number of interference fringes in the pattern of reflected light from a He-Ne laser (Ref. 29).

The growth system is an MO-CVD system with a vertical growth chamber. Upstream the prepurified hydrogen saturated with DES is mixed with hydrogen saturated with DEZ to form the adduct, $(C_2H_5)Zn \cdot Se(C_2H_5)$. The partial pressure of the DES is about twice that of the DEZ to insure that essentially all of the DEZ is bound up in the adduct. Six parts of H_2Se, which is in a 1.05% H_2Se mixture, is introduced immediately above the growth chamber to raise the Se:Zn ratio to 8:1. H_2Se is used because it can be obtained in purer form than the DES. The gas delivery rates and the growth rates are listed in Table 6, along with those of Stutius and Blanconnier, et al. The growth temperature was 500°C.

TABLE 6. THE GROWTH TEMPERATURE; DEZ, DMZ, H_2Se, DES, AND H_2 FLOW RATES; AND GROWTH RATE FOR CSU FILMS AND THOSE GROWN IN REFERENCES 25, 26, AND 27

| Sample | Growth T | Flow Rates - SCCM | | | | | Growth Rate μm/hr |
		DEZ	DMZ	H_2Se	DES	H_2	
Stutius	340°C	–	0.5	3	–	?	3-4
Blanconnier, et al	520°C	0.225-1.125	–	0.225-1.125	–	2300	0.6-4.8
CSU 1 on GaAs	500°C	–	0.2	2.4	0.8	1500	6.7
CSU 2 on GaAs	500°C	–	0.4	2.4	0.8	1500	15.0
CSU 3 on GaAs	500°C	–	0.8	2.4	0.8	1500	25.0
CSU 1 on glass	500°C	–	0.4	2.4	0.8	1500	1.5

Surface morphology of the films deposited on both GaAs and glass were examined by optical microscopy. In the former case the surface was smooth with occasional defects. In the latter, it appeared polycrystalline with a grain size the order of 1 μm. Adhesion of the film to glass, however, again exceeded the limit of our tester. The defects in the films on GaAs are thought to be precipitates from the adduct. A proposal to eliminate this problem is to cool the DES from room temperature to 0°C before it is introduced to the system and to dilute it further with additional H_2.

To qualitatively determine the crystal quality of the ZnSe on GaAs the (400) X-ray diffraction curve was obtained using a Lang camera. This type of camera uses a copper fine focus tube and a beam extender to yield high resolution diffraction peaks. The observed separation of the K_{α_1} and K_{α_2} lines for both the ZnSe and GaAs is a standard test of good crystalline quality.

The growth rates listed in Table 6 illustrate very well that the zinc delivery rate in our growth system is much higher when the zinc alkyl partial pressures are similar, probably due to less zinc being lost in room temperature precipitation reactions. The growth rate as seen in Table 6 is approximately linearly proportional to the zinc partial pressure, as

expected when there are no reactions competing with the deposition reaction. The lower growth rate on the glass substrate is probably due to the fundamental principle of growth kinetics that it is more difficult for a film to nucleate on an amorphous surface.

III. CONCLUSIONS

Thin films of SiO_2, Ta_2O_5, and TiO_2, deposited near room temperature by ion-beam-sputtering techniques, display several attractive features for optical coating applications. The lowest optical absorption coefficients have been 2.3 cm^{-1} for SiO_2, 3.9 cm^{-1} for Ta_2O_5, and 18 cm^{-1} for TiO_2. The films adhere well to quartz substrates, assuming a light predeposition sputter etch, and to each other in multilayer coatings. In both cases, the 10,000 psi (70 MPa) limit of the adhesion tester is exceeded. Indirect evidence for TiO_2 films, their near-bulk 2.50 ± 0.05 refractive index and lack of significant optical absorption change after baking, suggest they are dense and non-porous. Internal stress of the sputtered films is always compressive, near 0.5 GPa for Ta_2O_5 and TiO_2 films, about 1.0 GPa for SiO_2. The latter can be reduced somewhat by low energy ion bombardment of the substrate during deposition. Deposition rates are typically 60 Å/min.

Composition of the ion-beam-sputtered films, measured by XPS, is near stoichiometric when sufficient oxygen is added to the sputter beam (10% for an oxide target, 25% for an elemental target). A possible oxygen deficiency in the low absorption films of 1-2% is just at the resolution limit of the instrument. Similarly, the maximum concentration of the only observed chemical impurity, carbon, is also at the 1% resolution limit. Particulate contamination on the substrate can be reduced essentially to zero by using drag cleaning and clean room conditions. It invariably rises during deposition to the order of 50 visible defects/cm^2. Regions of the films near these visible defects were most susceptible to laser induced damage with a threshold near 5 J/cm^2. Regions free of visible defects showed a slightly higher threshold in TiO_2, and a significantly higher one, ~ 15 J/cm^2, in SiO_2 and Ta_2O_5.

Laser photodissociation of metal-carbonyls has shown that films of tungsten, molybdenum, and chromium with sound mechanical properties and reasonable visible reflectance can be deposited at 2000 Å/min at room temperature. As with the ion-beam-sputtered films, adhesion is near the limit of

34

the tester used. Stress, however, is tensile and the order of 0.5 GPa. Primary impurity is oxygen, approximately 7%, which is thought to result from residual O_2 in the deposition chamber.

Chemical vapor deposition at 500°C forms layers of ZnSe from a gas mixture of dimethylzinc, diethylselenide, and hydrogen selenide. Substrates of crystalline GaAs and amorphous glass were used. X-ray diffraction and surface morphology show a smooth, crystalline film forms on GaAs, a rough, probably polycrystalline film on glass.

Essentially all of the characterization done in the past year has been that of the macroscopic properties of the different types of deposited layers. The primary recommendation for the future is to add serious evaluation of the atomic level structure. Ultimately the optical and mechanical properties of thin films are determined by atomic bonding patterns in the bulk of the film, at the film-substrate interface, and for layered coatings at the interfaces between layers. Such studies should involve careful measurements of electron binding energies within an atom, and of bonding levels between atoms. The correlation between atomic structure and macroscopic characterization should be the key to the full evaluation of the different deposition processes.

REFERENCES

1. J.R. Sites, P. Gilstrap, and R. Rujkorakarn, Ion Beam Sputter Deposition of Optical Coatings, accepted by Optical Electronics and by NBS Special Publications for 1983 publication.

2. C.K. Carniglia, J.H. Apfel, T.H. Allen, T.A. Tuttle, W.H. Lowdermilk, D. Milam, and F. Rainer, NBS Special Publication #568, 359 (1979).

3. D.H. Gill, B.E. Newnam, and J. McLeod, NBS Special Publication #509, 260 (1977).

4. H.R. Kaufman, Technology of Electron Bombardment Ion Thrusters in Advances in Electronics and Electron Physics, Vol. 26, 265-373, L. Merton, Editor, Academic Press, New York, 1974.

5. Handbook of X-Ray Photoelectron Spectroscopy, G.E. Muilenberg, Ed., Perkin-Elmer Corporation, Eden Prairie, MN, 1979.

6. R.S. Robinson, Ph.D. Thesis, Colorado State University, 1978.

7. S.M. Rossnagel, P. Gilstrap, and R. Rujkorakarn, J. Vac. Sci. Technol. 21 (4), 1045 (1982).

8. J.A. Thornton, J. Tabock, and D.W. Hoffman, Thin Solid Films 64, 111 (1975).

9. A. Abeles, Ann. Phys. 5, 505 (1950).

10. R. Rujkorakarn, R.W. Hannum, and J.R. Sites, Reflectance Spectrum of Non-Optimum Multilayer Coatings, accepted by NBS Special Publications for 1983 publication.

11. R. Solanki, P.K. Boyer, and G.J. Collins, Appl. Phys. Lett. 41 (11), 1048 (1982).

12. G. Hass and L. Hadley in American Institute of Physics Handbook, Third Edition, 6-118, McGraw Hill, New York, 1972.

13. A.M. Ledger, Appl. Optics 18, 2979 (1979).

14. A.C. Papadopoulo, A.M. Jean-Louis, and J. Charil, J. Crystal Growth 44, 587 (1978).

15. S. Fujita, H. Mimoto, and T. Noguchi, J. Appl. Phys. 50, 1079 (1979).

16. X.W. Fan and J. Woods, IEEE Trans. Electron Dev. ED-28, 428 (1981).

17. N.T. Gordon, IEEE Trans. Electron Dev. ED-28, 434 (1981).

18. A.M. Goodman, J. Electrochem. Soc. 116, 364 (1969).

19. M.R. Czerniak and P. Lilley, J. Crystal Growth 59, 455 (1982).

20. W.M. Yim and E.J. Stofko, J. Electrochem. Soc. 119, 381 (1972).

21. K.L. Lewis, D.J. Cook, and P.B. Roscoe, J. Crystal Growth 56, 614 (1982).

22. H. Hartmann, J. Crystal Growth 42, 144 (1977).

23. A.V. Simashkevich and R.L. Tsiulyanu, J. Crystal Growth 35, 369 (1976).

24. T. Niina, T. Minato, and K. Yoneda, Jap. J. Appl. Phys. 21, L387 (1982).

25. P. Blanconnier, M. Cerclet, P. Henoc, and A.M. Jean-Louis, Thin Solid Films 55, 375 (1978).

26. W. Stutius, Appl. Phys. Lett. 33, 656 (1978).

27. W. Stutius, J. Electronic Mat. 10, 95 (1981).

28. J.B. Mullin, S.J.C. Irvine, and D.J. Ashen, J. Crystal Growth 55, 92 (1981).

29. Handbook of Thin Film Technology, L.I. Maissel and R. Glang, ed., pp. 12-22, McGraw Hill, New York, 1970.

BASIC LANGUAGE COMPUTER PROGRAM

FOR REFLECTIVITY CALCULATIONS

```
10   REM : OPTIC2
20   REM : THIS PROGRAM CALCULATE
     S, STORES, AND GRAPHS THE RE
     FLECTIVITY FOR 3 OR 15 FILM
     LAYERS.
30   REM : THE FILM THICKNESS, RE
     FRACTIVE INDEX, AND EXTINCTI
     ON COEFFICIENT MAY BE VARIED
40   REM : VARIABLE DECLARATION
50   INTEGER M,Z1,B,J,J1,I,Z,Y
60   SHORT N1,N2,K,X,L,X1,X2,S1,Y
     1,Y2,S2
70   DIM D(16),N(16),K(16),P(16),
     Q(16),R(16),S(16),T(16),U(16
     ),V(16),W(16),R1(260)
80   REM : MAIN PROGRAM
90   GOSUB 310
100  REM : CALL ROUTINES TO COMPU
     TE AND STORE NORMAL REFLECTI
     VITY AND TRANSMISSION
110  IF N$="N" THEN 170
120  B=1
130  GOSUB 1120
140  GOSUB 1320
150  ASSIGN# 1 TO *
160  REM : CALL ROUTINES TO COMPU
     TE VARIATIONS
170  B=2
180  IF A$="Y" THEN GOSUB 770
190  IF B$="Y" THEN GOSUB 870
200  IF C$="Y" THEN GOSUB 1010
210  IF G$="N" THEN 280
220  ASSIGN# 2 TO *
230  ASSIGN# 1 TO D1$
240  ASSIGN# 2 TO D2$
250  REM : CALL ROUTINE TO GENERA
     TE GRAPHS
260  GOSUB 1730
270  ASSIGN# 1 TO *
280  ASSIGN# 2 TO *
290  STOP
300  REM : INPUT PROGRAM PARAMETE
     RS SUBROUTINE
310  Y=0
320  CLEAR
330  DISP "ENTER THE NUMBER OF FI
     LM LAYERS"
340  INPUT M
350  DISP "ENTER THE HIGH REFRACT
     IVE INDEX"
360  INPUT N1
370  DISP "ENTER THE LOW REFRACTI
     VE INDEX"
380  INPUT N2
390  DISP "ENTER THE EXTINCTION C
     OEFIFICENT MULTIPLIER (e.g.
     0 OR 10E-2)"
400  INPUT K
410  DISP "COMPUTE AND STORE NORM
     AL REFLECTIVITY Y/N"
420  INPUT N$
430  DISP "VARY FILM THICKNESS Y/
     N"
440  INPUT A$
450  DISP "VARY THE REFRACTIVE IN
     DEX Y/N"
460  INPUT B$
470  DISP "VARY THE EXTINCTION CO
     EFFICIENT Y/N"
480  INPUT C$
490  REM : CREATE DATA FILE SUBRO
     UTINE
500  DISP "ENTER THE DATA FILE AN
     D VOLUME FOR NORMAL REFLECTI
     VTY (e.g. MUL1.OPST2)"
510  INPUT D1$
520  IF N$="N" THEN 540
530  CREATE D1$,1,2088
540  ASSIGN# 1 to D1$
550  DISP "ENTER THE DATA FILE AN
     D VOLUME FOR VARIATIONS (e.g.
     . MUL3.OPST2)"
560  INPUT D2$
570  DISP "ENTER THE NUMBER OF RE
     CORDS (e.g. 14 FOR ALL VARIA
     TIONS)"
```

```
580   INPUT 21
590   CREATE D2$,Z1,2088
600   ASSIGN# 2 TO D2$
610   REM : INPUT GRAPH PARAMETERS
       SUBROUTINE
620   DISP "GENERATE GRAPHS Y/N"
630   INPUT G$
640   IF G$="N" THEN 750
650   DISP "PRINT SEPARATE GRAPH O
       F NORMAL REFLECTIVITY Y/N"
660   INPUT S$
670   DISP "ENTER THE X-AXIS ORIGI
       N AND MAXIMUM VALUE (e.g. .4
       ,3 μm)"
680   INPUT X1,X2
690   DISP "ENTER THE X-AXIS TIC S
       PACING INTERVAL (e.g. .4)"
700   INPUT S1
710   DISP "ENTER THE Y-AXIS ORIGI
       N AND MAXIMUM VALUE (e.g. 0,
       1; 1=100%)"
720   INPUT Y1,Y2
730   DISP "ENTER THE Y-AXIS TIC S
       PACING INTERVAL (e.g. .1)"
740   INPUT S2
750   RETURN
760   REM : FILM THICKNESS VARIATI
       ON SUBROUTINE
770   GOSUB 1120
780   FOR Z=1 TO 3
790   FOR X-.8 TO 1.2 STEP .4
800   D(Z) = 1.06*X/(4*N(Z))
810   GOSUB 1320
820   NEXT X
830   D(Z)=1.06/(4*N(Z))
840   NEXT Z
850   RETURN
860   REM : REFRACTIVE INDEX VARIA
       TION SUBROUTINE
870   GOSUB 1120
880   FOR Z=1 TO 3
890   FOR X=.8 TO 1.2 STEP .4
900   IF Z=1 THEN N(1)=N1*X
910   IF Z=2 THEN N(2)=N2*X
920   IF Z=3 THEN N(3)-N1*X
930   D(Z)=1.06/(4*N(Z))
940   GOSUB 1320
950   NEXT X
960   N(1),N(3)=N1 @ N(2)=N2
970   D(Z)=1.06/(4*N(Z))
980   NEXT Z
990   RETURN

1000  REM : EXTINCTION COEFFICIEN
       T VARIATION SUBROUTINE
1010  DATA .005, .01
1020  GOSUB 1120
1030  FOR Z=1 TO 2
1040  READ K
1050  FOR J=1 TO M+1
1060  K(J)=K
1070  NEXT J
1080  GOSUB 1320
1090  NEXT Z
1100  RETURN
1110  REM : INITIALIZE VARIABLES
       SUBROUTINE
1120  D(0)=0
1130  D(M+1)=0
1140  K(0)=0
1150  N(0)=1
1160  N(M+1)=1.5
1170  FOR J=1 TO M STEP 2
1180  N(J)=N1
1190  NEXT J
1200  FOR J=2 TO M STEP 2
1210  N(J)=N2
1220  NEXT J
1230  FOR J=1 TO M+1
1240  K(J)=K
1250  NEXT J
1260  FOR J=1 TO M
1270  D(J)=1.06/(4*N(J))
1280  NEXT J
1290  RETURN
1300  REM : CALCULATE AND STORE T
       HE REFLECTIVITY SUBROUTINE
1310  REM : COMPUTE INDIVIDUAL MA
       TRICES
1320  I=0
1330  FOR L=.4 TO 3 STEP .01
1340  FOR J=1 TO M+1
1350  J1=J-1
1360  A=2*PI*K(J1)*D(J1)/L
1370  C=2*PI*N(J1)*D(J1)/L
1380  P=EXP(A)*COS(C)
1390  Q=EXP(A)*SIN(C)
1400  G=(N(J1)^2+K(J1)^2-N(J)^2-K
       (J)^2)/((N(J1)+N(J))^2+(K(J
       1)+K(J))^2)
1410  H=2*(N(J1)*K(J)-N(J)*K(J1))
       /((N(J1)+N(J))^2+(K(J1)+K(J
       ))^2)
1420  R=EXP(A)*(G*COS(C)-H*SIN(C)
       )
```

```
1430  S=EXP(A)*(H*COS(C)+G*SIN(C)
      )
1440  T=EXP(-A)*(G*COS(C)+H*SIN(C
      ))
1450  U=EXP(-A)*(H*COS(C)-G*SIN(C
      ))
1460  V=EXP(-A)*COS(C)
1470  W=-(EXP(-A)*SIN(C))
1480  REM : COMPUTE THE MATRIX PR
      ODUCT
1490  IF J<>1 THEN 1550
1500  P(1)=P @ Q(1)=Q
1510  R(1)=R @ S(1)=S
1520  T(1)=T @ U(1)=U
1530  V(1)=V @ W(1)=W
1540  GOTO 1630
1550  P(J)=P(J1)*P-Q(J1)*Q+R(J1)*
      T-S(J1)*U
1560  Q(J)=Q(J1)*P+P(J1)*Q+S(J1)*
      T+R(J1)*U
1570  R(J)=P(J1)*R-Q(J1)*S+R(J1)*
      V-S(J1)*W
1580  S(J)=Q(J1)*R+P(J1)*S+S(J1)*
      V+R(J1)*W
1590  T(J)=T(J1)*P-U(J1)*Q+V(J1)*
      T-W(J1)*U
1600  U(J)=U(J1)*P+T(J1)*Q+W(J1)*
      T+V(J1)*U
1610  V(J)=T(J1)*R-U(J1)*S+V(J1)*
      V-W(J1)*W
1620  W(J)=U(J1)*R+T(J1)*S+W(J1)*
      V+V(J1)*W
1630  NEXT J
1640  J1=J-1
1650  A1=P(J1)^2+Q(J1)^2
1660  R1(I)=(T(J1)^2+U(J1)^2)/A1
1670  I=I+1
1680  NEXT L
1690  Y=Y+1
1700  PRINT # B,Y ; R1()
1710  RETURN
1720  REM : PRINT GRAPHS SUBROUTI
      NE
1730  X=1
1740  Z=2
1750  GOSUB 1940
1760  READ* 1,1 ; R1()
1770  GOSUB 2280
1780  IF S$="N" THEN 1830
1790  COPY
1800  PRINT USING "5/"

1810  S$="N"
1820  IF Y=1 THEN 1920 ELSE 1750
1830  FOR J=X TO Z
1840  READ# 2,J ; R1()
1850  GOSUB 2280
1860  NEXT J
1870  COPY
1880  PRINT USING "5/"
1890  X=X+2
1900  Z=Z+2
1910  IF J<Y THEN 1750
1920  RETURN
1930  REM : GRAPH SET-UP SUBROUTI
      NE
1940  GCLEAR
1950  LOCATE 13,133,7,100
1960  SCALE X1,X2,Y1,Y2
1970  XAXIS Y1,S1,X1,X2
1980  YAXIS X1,S2,Y1,Y2
1990  XAXIS Y2,X2,X1,X2
2000  YAXIS X2,Y2,Y1,Y2
2010  LDIR 0
2020  LORG 1
2030  SETGU
2040  MOVE 98,94
2050  LABEL USING "2A,K" ; "M=",M
2060  LABEL USING 2090 ; "Nh=",N1
2070  LABEL USING 2090 ; "N1=",N2
2080  LABEL USING 2090 ; "Ns=",N(
      M+1)
2090  IMAGE 3A,D.DD
2100  MOVE 9,0
2110  LABEL X1
2120  MOVE 62,0
2130  LABEL "λ (μm)"
2140  MOVE 136,0
2150  LORG 7
2160  LABEL X2
2170  MOVE 15,6
2180  LABEL Y1*100
2190  MOVE 12,47
2200  LABEL "(%)"
2210  MOVE 8,56
2220  LABEL "R"
2230  MOVE 16,95
2240  LABEL Y2*100
2250  SETUU
2260  RETURN
2270  REM : DRAW REFLECTIVITY SUB
      ROUTINE
2280  L=.4
```

41

```
2290   FOR I=0 TO 260
2300   IF L<=X1 THEN MOVE L,R1(I)
       ELSE DRAW L,R1(I)
2310   L=L+.01
2320   NEXT I
2330   RETURN
2340   END
```

END

FILMED

9-83

DTIC